Cellulose (2024) 31:9699–9713
https://doi.org/10.1007/s10570-024-06191-2

ORIGINAL RESEARCH

Cellulose nanofiber aerogels: effect of the composition and the drying method

Farida Baraka · Kathirvel Ganesan · Barbara Milow · Jalel Labidi

Received: 19 April 2024 / Accepted: 24 September 2024 / Published online: 4 October 2024

Abstract Highly porous and lightweight aerogels of cellulose nanofibers (CNFs) have emerged as a promising class of material. This study delves into the impact of the composition (lignocellulose nanofibers–LCNFs and CNFs) and the drying methods (supercritical drying and freeze-drying) on the morphology and the properties of nanocellulose-based aerogels. The investigation evaluates the concentrations of nanofibers and the influence of lignin, a constituent of LCNFs recognized for enhancing the rigidity of plant cell walls, on the aerogel's properties. The shrinkage rates, density, pore structure, and mechanical properties of the obtained aerogels are comprehensively compared. Supercritical drying proves advantageous for aerogel formation, resulting in materials with lower density and higher surface area than their freeze-dried counterparts at each concentration level. The use of acetone for supercritical drying contributes to reduce the shrinkage rates compared to ethanol. This decrease is attributed to the formation of a more rigid hydrogel during solvent exchange. Freeze-drying exhibits the lowest shrinkage rates and relatively higher porosity. The presence of lignin in the nanofibers influences the microstructure, yielding smoother and thicker pore walls. This study contributes to the comprehensive understanding of the intricate factors shaping nanocellulose aerogel properties, paving the way for the development of innovative and environmentally-friendly materials.

Keywords Cellulose nanofibers · Lignocellulose · Aerogels · Freeze-drying · Supercritical drying

Supplementary Information The online version contains supplementary material available at https://doi.org/10.1007/s10570-024-06191-2.

F. Baraka · J. Labidi (✉)
Biorefinery Processes Group, Chemical and Environmental Engineering Department, Engineering Faculty of Gipuzkoa, University of the Basque Country UPV/EHU, Plaza Europa 1, 20018 Donostia-San Sebastián, Spain
e-mail: jalel.labidi@ehu.eus

K. Ganesan · B. Milow (✉)
German Aerospace Center (DLR), Institute of Materials Research, Aerogels and Aerogel Composites, 51147 Cologne, Germany
e-mail: barbara.milow@dlr.de

B. Milow
Department of Chemistry, Nanostructured Cellular Materials, University of Cologne (UoC), 50939 Cologne, Germany

Introduction

As the most abundant, biocompatible, and biodegradable biopolymer on Earth, cellulose represents a promising raw material to replace polymers derived from fossil resources (Mankar et al. 2021). This versatility provides considerable potential for the development of innovative and high value-added materials, especially aerogels (García-González et al. 2011,

2015; Wang et al. 2019; Verma et al. 2020). Pioneered by Kistler (1931), aerogels are porous materials obtained by replacing the liquid component of a gel with air while maintaining their three-dimensional network structure. These materials exhibit unique characteristics such as high porosity, large specific surface area, low density, low thermal conductivity, and low dielectric constant; among others (Pierre and Pajonk 2002; Keshavarz et al. 2021; Tafreshi et al. 2022; Steiner et al. 2023). Combining these properties with those of cellulose offers considerable potential for developing innovative, lightweight, and environmentally-friendly materials covering a wide range of applications (Ganesan et al. 2016; Illera et al. 2018; Wei et al. 2020; Ho and Leo 2021; Chen et al. 2021; Sepahvand et al. 2023).

Nanocellulose-based aerogels are an emerging subclass of aerogels composed of cellulosic materials with a dimension in the nanometer range. These aerogels combine the unique properties of cellulose with the specific characteristics of nanoscale materials (Dufresne 2019). They can be produced using various nanoscale fibrillar crystalline domains extracted from various types of cellulose (Ho and Leo 2021). These domains are commonly classified into three primary groups based on their distinct compositions and their extraction methods: cellulose nanofibers (CNFs), cellulose nanocrystals (CNCs), and bacterial nanocellulose (Kargarzadeh et al. 2018). The structure and the morphology of nanocellulose play a significant influence on the method of hydrogel gelation; which can, in term, have a significant impact on the aerogel's properties (De France et al. 2017). Furthermore, the selection of an appropriate drying method to minimize the collapse of the network structure is of crucial importance (Buchtová and Budtova 2016; Ganesan et al. 2016). This determining step influences the morphology of the material and confers distinctive characteristics to the nanocellulose-based aerogels, while preserving their structural integrity (Chen et al. 2013; Husain et al. 2021).

Cellulose nanofiber aerogels were designed for the first time by Pääkkö et al. using the freeze-drying method (Pääkkö et al. 2008). This process involves the sublimation of a solid, usually frozen water, filling the pores of nanocellulose hydrogel. In their study, the impact of the freeze-drying techniques, i.e. cryogenic and vacuum freeze-drying, on the aerogel's properties was explored. Both approaches led to the formation of CNF aerogels with low density and high porosity. The specific surface area was dependent on the drying techniques with higher values reported for the cryogenic freeze-drying. Later, Ciftci et al. further investigated the properties of CNF aerogels prepared from physically cross-linked hydrogels that were subjected to freeze drying or supercritical drying (Ciftci et al. 2017). Supercritical carbon dioxide (Sc–CO_2) drying involves the elimination of liquid/gas surface tension to achieve a state of zero liquid/gas surface tension (García-González et al. 2012). This methodology proved to effectively preserve the aerogel's porous structure with a higher specific surface area compared to those prepared via the freeze-drying technique. The lower density was attributed to the sublimation of water crystals during freeze-drying, leading to the disruption of the porous structure. In an attempt to mitigate this undesirable effect, other studies have explored incorporating cellulose nanofibers containing lignin fractions (Morcillo-Martín et al. 2022). Lignin, an aromatic biopolymer, characterized by a heterogenous cross-linked network, forms complexes with cellulose via hydrogen bonding and covalent linking (Rojo et al. 2015; Morales et al. 2021). The unique aromatic structure of lignin confers impermeability, enhances structural integrity, and imparts rigidity to plants. Additionally, its phenolic moieties offer antimicrobial and antioxidant properties, preventing degradation (Adjaoud et al. 2021). Lignocellulose nanofibers (LCNFs) can be obtained using various methods (Jiang et al. 2021). Among them, mechanical treatment of unbleached cellulose pulp is a common approach (Visanko et al. 2017). Other effective methods include acid hydrolysis, which uses specific acids such as formic acid, maleic acid, oxalic acid, thus preserving lignin fractions (Liu et al. 2021). More recently, deep eutectic solvent (DES) treatment has emerged as a promising method to extract LNCFs (Fu et al. 2022). It enables a controlled extraction by precisely adjusting the extraction time and temperature, which can result in a variation in the lignin fraction. The presence of lignin on the surface of nanofibers brings significant benefits, beyond simply reducing environmental impact and production costs. Owing to its high concentration of non-polar hydrocarbon and benzene groups, lignin confers enhanced hydrophobicity, increases thermal stability, and improves the mechanical properties of nanocellulose (Herrera et al. 2018; Tanguy et al. 2021). Thus, incorporating lignin

into nanocellulose aerogel could potentially reduce the negative impacts of the freeze-drying method by enhancing the mechanical properties of the resulting aerogels, particularly their strength and rigidity. Furthermore, aerogels derived from LCNFs demonstrate an even higher specific surface area. The origin of this improvement has not been clearly interpreted and linked to the presence of lignin. It is also noteworthy to mention that this specific surface value is the highest reported when freeze-drying is applied as the drying method. This innovative approach underlines the fundamental importance of nanocellulose aerogel composition in shaping their ultimate properties.

Nevertheless, the potential influence of lignin on the characteristics of aerogels produced by supercritical drying remains to be elucidated. During this process, pressure is increased to reach supercritical conditions, a factor that could potentially induce aerogel shrinkage. Inspired by these pioneering works and to address these inquiries, the aim of the present study was to further investigate the influence of nanocellulose composition. Several aspects were explored including the lignin content and nanofiber concentration, as well as the impact of the drying method on the morphology and the properties of nanocellulose aerogels. This study aimed to determine whether partial removal of lignin during extraction could lead to nanocellulose aerogels with improved porous morphology and mechanical properties. Nanocellulose aerogels were synthesized from the freeze-thaw physical cross-linking of hydrogels that were subjected to two distinct drying methods: freeze-drying and supercritical drying. The resulting aerogels have been characterized and compared in terms of their shrinkage rate, density, pore structure, and mechanical properties. Finally, this comparative study intends to provide a comprehensive overview of the nanocellulose aerogels obtained by the two drying methods, while highlighting the potential influence of lignin on the material's final properties.

Experimental methods

Materials

Lignocellulose and cellulose nanofibers, designated as LCNFs and CNFs, respectively, were extracted from Eucalyptus cellulose pulp through a homogenization process. The used extraction method was described in our previous publication (Baraka et al. 2023). Detailed analyses of their chemical composition and structural characteristics are provided in Table 1.

Hydrogel synthesis

Hydrogels were synthesized via physical crosslinking involving the freeze-thawing of water suspensions containing different concentrations of nanofibers (1%, 1.5%, and 2% by weight). Initially, mechanically extracted nanofibers were centrifuged at 8000 rpm for 10 min. The resulting pulp was dispersed in distilled water using an UltraTurrax high-shear homogenizer (IKA® T25 digital), operating at 10,000 rpm for 5 min. To eliminate air bubbles, the suspensions were treated for 1 min in an ultrasonic bath. The resulting suspensions were then poured into polypropylene cups and placed in a freezer at −20 °C for 12 h. The gradual thawing process took place in a refrigerator at 4 °C for 12 h, enabling the formation of physically cross-linked hydrogels. This cross-linking results from the crystallization of water molecules present in the nanofiber suspension during the freezing process. The water crystals reduce the space between nanocellulose chains, favouring areas of higher concentration. This proximity between the chains encourages the formation of hydrogen bonds between the nanofibers, acting as physical cross-linking points and leading to the creation of a three-dimensional network.

Table 1 Composition and structural properties of lignocellulose nanofibers (LCNFs) and cellulose nanofibers (CNFs)

		LCNFs	CNFs
Composition (%)[a]	Ashes	0.64 ± 0.05	0.91 ± 0.12
	Extractives	1.56 ± 0.16	0.25 ± 0.0.83
	Lignin	7.33 ± 0.20	2.33 ± 0.16
	Hemicellulose	23.39 ± 0.15	26.96 ± 0.27
	Cellulose	66.89 ± 0.66	72.32 ± 0.07
Crystallinity (%)[b]		62.51	60.68
Diameter (nm)[c]		11.79 ± 2.54	16.98 ± 2.95

[a]Determined following TAPPI T211, T204, T222, T204

[b]Determined by X-ray diffraction analysis following the peak deconvolution method (Park et al. 2010)

[c]The diameters of cellulose nanofibers were measured by analysing scanning electron microscope images

Supercritical drying

Aerogels were produced from nanocellulose hydrogels by solvent exchange using two different organic solvents. The substitution of water by an organic solvent, essential to prevent alteration during supercritical drying, can induce variable shrinkage depending on the solvent used (Raman et al. 2019). The volume shrinkage (Eq. 1), defined as the difference between the initial alcogel volume (V_i) and the final aerogel volume (V_f) relative to the initial volume, can vary. The cross-linking of cellulose nanofiber hydrogels relies on hydrogen bonds, which can be altered during this solvent exchange, affecting the porous structure of the resulting aerogels. Thus, the effects of solvent exchange on the properties of cellulose nanofiber aerogels obtained after supercritical drying were investigated using acetone and ethanol.

$$\text{Volume shrinkage}(\%) = \frac{(V_f - V_i)}{V_i} \times 100 \quad (1)$$

Sc–CO_2 drying was carried out by placing the nanocellulose alcogels in an autoclave (HPTE-150p, 60L) containing pure CO_2 with a flow rate of 25 kg/h, at a temperature of 60 °C and a pressure ranging from 110 to 115 bar depending on the organic solvent used. The labels of the aerogels obtained are presented in Table 2 and vary according to composition, nanofiber concentration, organic solvent, and drying method.

Freeze-drying

To produce aerogels by freeze-drying, nanocellulose hydrogels were frozen at −20 °C for 24 h prior to the lyophilization process. Subsequently, the ice present in the frozen hydrogel was sublimated under vacuum using a CHRIST Alpha 2–4 LSC freeze-dryer, at a condensation temperature of −110 °C, over a period of 72 h. The labels of the aerogels obtained are listed in Table 2, according to composition, nanofiber concentration and drying method.

Table 2 Aerogels labeled according to their composition, nanofiber concentration, organic solvent, and drying method

Samples label (x =1, 1.5, 2)[a]	Composition		Drying method		
	Cellulose nanofibers	Lignocellulose nanofibers	Sc–CO_2 ethanol[b]	Sc–CO_2 acetone[c]	FD[d]
AECNFx	x		x		
AELCNFx		x	x		
AACNFx	x			x	
AALCNFx		x		x	
AFCNFx	x				x
AFLCNFx		x			x

[a]Concentrations of nanofibers (wt.%)

[b]Supercritical drying using ethanol for the solvent exchange process

[c]Supercritical drying using acetone for the solvent exchange process

[d]Freeze-drying

Aerogel characterization

Bulk density

The bulk density (ρ_e) of the aerogels was measured using the Micromeritics GeoPyc 1360. For reliable measurements, each sample was subjected to three measurement cycles, with a constant force of 35N applied during each cycle.

Skeletal density

The skeletal density (ρ_s) of the samples was characterized by using Micromeritics Accupyc II 1320 (helium gas). The volume of the sample carrier was 1 cm^3. The helium gas pycnometer provided a precise volume of sample. With the known value of mass, the data yielded the skeletal density of various samples. In order to avoid the influence of porous structures, all the samples were crushed to film like sheets and then the analysis was carried out. Independent of the compositions of samples and the drying techniques, the value of skeletal density for all the samples was in the range between 1.5825 and 1.6001 g/cm^3. An average skeletal density of 1.5917 ± 0.0073 g/cm3 was used for further porosity analysis.

Porosity

The porosity was calculated as follows (Eq. 2):

$$\text{Porosity } (\%) = 1 - \frac{\rho_e}{\rho_s} \quad (2)$$

where ρ_e is attributed to the bulk density and ρ_s to the skeletal density.

Specific surface area

The specific surface area measurements using the Brunauer–Emmett–Teller (BET) method and pore size characterization using the Barrett–Joyner–Halenda (BJH) method were carried out on nanocellulose aerogels. These analyses were carried out via low-temperature nitrogen adsorption-desorption using a Micromeritics–Tristar II 3020 instrument, for the aerogels obtained by supercritical drying. For the nanocellulose aerogels prepared by freeze-drying, their specific surface area was determined by the krypton adsorption method using the Micromeritics–3Flex instrument. This method was applied in view of their low specific surface area (< 10 m^2/g). For each analysis, a small amount of aerogel samples (around 1 mg) was placed in the sample tube, then subjected to a vacuum degassing process at 120 °C for 3 h prior to analysis, ensuring water and gases desorption for reliable results.

Scanning electron microscopy (SEM)

To assess the pore shape and interconnected network structures of the nanocellulose aerogels, the latter were analyzed using a Merlin—Carl Zeiss Scanning Electron Microscope (SEM). Prior to imaging, the aerogel samples were sputter-coated with a thin layer of gold. Cross-sections were examined to obtain a detailed view of the aerogels' three-dimensional structure.

Compression test

The compression performance of the nanocellulose aerogels was evaluated using uniaxial compression tests on a ZwickRoell Z2.5 machine equipped with a 50N load cell. Due to their irregular shape, attributable to shrinkage during drying, evaluation required adjustment of the machine's top plate to align the tops of the aerogel samples and make their upper surface perfectly flat. The samples were compressed at a traverse speed of 5 mm/min until they reached 80% of their initial thickness. Compressive modulus was determined by analyzing the slope of the stress-strain curve in the linear range.

Results and discussion

Aerogels appearance and shrinkage rate

The aerogels were produced by the gradual thawing of nanocellulose suspension to allow the formation of physically cross-linked hydrogels. The process took place in a refrigerator at 4 °C for 12 h. The cross-linking results from the crystallization of the water present in the nanofiber suspension during the freezing process. The water crystals reduce the space between nanocellulose chains, favouring areas of higher concentration. This proximity between the chains encourages the formation of hydrogen bonds between the nanofibers, acting as physical cross-linking points and leading to the creation of a three-dimensional network.

Illustrated in Fig. S2, the aerogels obtained from various drying processes display significant variations in terms of shape and color. Aerogels derived from cellulose nanofibers (CNFs) are characterized by a white shade. Conversely, the shade of aerogels made from lignocellulose nanofibers (LCNFs) tends towards brown tones, attributed to the presence of lignin fractions. Regarding the shapes of the aerogels obtained, whether they are regular or marked by a certain shrinkage, they are closely dependent on the initial concentration of nanocellulose, their composition, and the drying method.

Nanocellulose suspensions, with concentrations ranging from 1 to 2 wt.%, have been employed in the preparation of nanocellulose-based aerogels. It is important to note that hydrogels cannot be formed from solutions with a lower nanocellulose content. Indeed, the formation of the interconnected network relies essentially on hydrogen-bond interactions between the cellulose chains. At lower concentrations, the hydrogen-bond interaction appears insufficient to induce stable hydrogel formation. Crucially,

increasing the concentration of nanofibers leads to a substantial increase in the rigidity of the resulting hydrogel. Indeed, a higher concentration of nanofibers in the suspension induces multiplication of physical cross-linking points, thus favouring the constitution of a stable and rigid hydrogel. In contrast, suspensions of lignocellulose nanofibers produced less rigid hydrogels. This disparity can be attributed to a reduction in hydrogen bonding interactions, probably due to the presence of aromatic groups from the lignin fractions. These aromatic groups reduce interactions between nanofibers, hindering the formation of tightly interconnected networks. This observation becomes particularly striking during the drying process. As evidenced in Fig. S2, LCNF aerogels obtained at lower concentrations reveal irregular structures, attesting to the significant shrinkage.

The evolution of the volume shrinkage of aerogels obtained by different drying methods is illustrated in Fig. 1. Drying with supercritical CO_2 generates a significant volumetric shrinkage, which decreases with a higher content of nanofibers (Ciftci et al. 2017). Higher concentrations of nanofibers confer enhanced rigidity to the material. As the concentration rises, the nanofibers form a more closely interconnected network, reinforcing the overall structure. Thus, the reinforced presence of nanofibers acts as a counterbalance to capillary forces contributing to shrinkage, promoting a more stabilized structure and reduced shrinkage. Similarly, the formation of a network composed of lignocellulose nanofibers results in a less interconnected and less rigid structure, thus leading to a higher shrinkage rate. However, the shrinkage rate is notably reduced in aerogels subjected to solvent exchange with acetone, despite its lower interfacial surface tension compared to ethanol. This noteworthy reduction in shrinkage can be attributed to the development of a more rigid hydrogel during the solvent exchange process. Acetone, classified as a polar aprotic solvent, has the capability to induce more interactions with cellulose nanofibers embedded within the hydrogel matrix. These enhanced hydrogen bonding promote the creation of a denser and more rigid structure. In addition, a lower pressure (100 bar) is employed during the supercritical drying process when using acetone rather than ethanol (115 bar). This pressure difference may also have influenced the final properties of the nanocellulose-based aerogels. Lower pressure may help to preserve the hydrogel's three-dimensional structure, thereby reducing the rate of shrinkage.

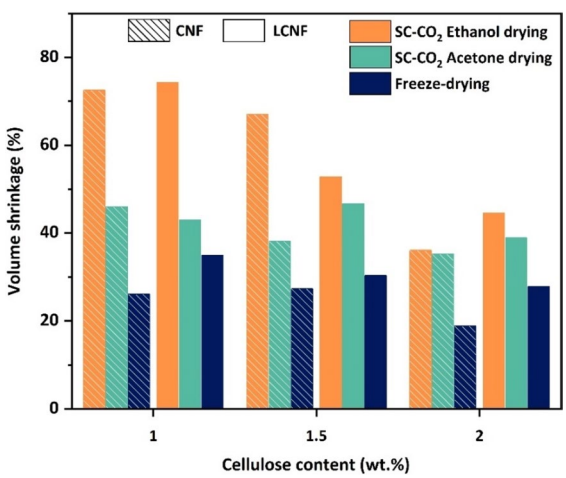

Fig. 1 Evolution of the volume shrinkage of aerogels obtained from various drying methods as a function of nanocellulose concentration

Freeze-drying generates the lowest volume shrinkage as compared with supercritical drying. In contrast to the other samples, the volumetric shrinkage of both types of aerogels did not exceed 30% as reported by (Buchtová et al. 2019), but seemed to follow the same trend with increasing nanocellulose concentration. Additionally, the freeze-drying method ensures the relatively regular appearance of the aerogel. As the solvent passes directly from the solid to the gaseous state, disruption of the material structure is minimized, resulting in less pronounced overall shrinkage.

Aerogel density and porosity

The bulk density of nanocellulose aerogels and their porosity are summarized in Table 3. Predictably, the bulk density of the samples increases proportionally with nanocellulose concentration. This value includes the entire density of the aerogel, encompassing both the solid material formed of nanofibers and the voids present within its structure. As the mass concentration of nanofibers increases, a simultaneous increase in bulk density is observed. It was with an exception for the bulk density of AECNF 2 wt.% (0.0178 g/cm^3) which was equal to AECNF1.5 wt.% due to the less volume shrinkage of 2 wt.%. Regardless of the cellulose and lignin concentrations, aerogel compositions,

Table 3 Total volume shrinkage, bulk density, skeletal density, and porosity of nanocellulose-based aerogels

Sample	Nanocellulose concentration (wt.%)	Volume shrinkage (%)	Bulk density (g cm^{-3})	Porosity (%)	BET specific surface area (m^2 g^{-1})	Pore volume* (cm^3 g^{-1})
AACNF	1	45.98	0.0125	99.215	81.67	0.2825
	1.5	38.14	0.0138	99.133	79.12	0.2808
	2	35.25	0.0146	99.083	69.14	0.2735
AALCNF	1	42.93	0.0138	99.133	78.26	0.3454
	1.5	46.64	0.0151	99.051	71.84	0.2993
	2	38.90	0.0191	98.800	80.32	0.3560
AECNF	1	72.52	0.0127	99.202	105.15	0.4222
	1.5	67.03	0.0178	98.882	87.01	0.3135
	2	36.06	0.0178	98.882	68.78	0.2341
AELCNF	1	74.25	0.0120	99.246	84.99	0.4838
	1.5	52.75	0.0143	99.102	86.44	0.3521
	2	44.56	0.0177	98.888	76.11	0.3311
AFCNF	1	26.11	0.0108	99.321	5.16	0.0061
	1.5	27.35	0.0115	99.215	4.27	0.0021
	2	18.86	0.0132	99.171	3.71	0.0027
AFLCNF	1	34.98	0.0113	99.290	5.98	0.0029
	1.5	30.36	0.0116	99.259	5.02	0.0016
	2	27.81	0.0149	99.064	4.48	0.0007

*Determined from the point absorption at a relative pressure of 0.99 in Kr isotherms

Determined from BJH Desorption cumulative volume of pores between 1.7000 nm and 300.0000 nm diameter in N_2 isotherms

or drying conditions, the average skeletal density was consistently measured at 1.5917 ± 0.0073 g/cm^3. This value aligns closely with those reported in the literature, where the addition of lignin, even at high concentrations (up to 12 wt.%), has no significant effect on skeletal density (Daicho et al. 2020).

The porosity of the different aerogels is highly dependent on the nanofiber concentration and the drying method. Indeed, for an aerogel containing similar concentration of nanofibers but synthesized using different drying methods, it can be observed that the porosity slightly increases with decreasing shrinkage rate. This trend is particularly noticeable in the 2 wt.% CNF aerogels. Indeed, the porosity of an aerogel describes the ratio of empty space (or pores) within its structure to its overall volume. Thus, if an aerogel undergoes less shrinkage during the drying process, leading to an increase in its apparent volume and porous volume (as shown in Table 2), this ultimately leads to an increase in its porosity (Ciftci et al. 2017). Due to the very low volume contraction during freeze-drying, AFCNF2% aerogels exhibit the higher porosity compared with the AECNF2% aerogel dried using supercritical drying with ethanol solvent exchange, thus inducing higher shrinkage.

However, by comparing batches of aerogels synthesized with the same drying method, another correlation is revealed: as the nanofiber mass concentration increases, the shrinkage rate decreases, but simultaneously, the porosity rate also decreases (Ciftci et al. 2017; Zhu et al. 2021). This observation is clearly illustrated in the case of aerogels prepared by supercritical acetone drying, where porosity drops from 99.167% for AACNF 1% to 99.027% for AACNF 2%. This tendency can be explained by the thickening of pore walls with increasing nanofiber concentration, leading to a reduction in the available pore space as observed by Ciftci et al. 2017. Indeed, the closer interaction between nanofibers can induce the formation of denser structures, thus influencing the porous properties of aerogels.

Specific surface area and pore size

The evaluation of the porous properties, including specific surface area and volume pores, was carried

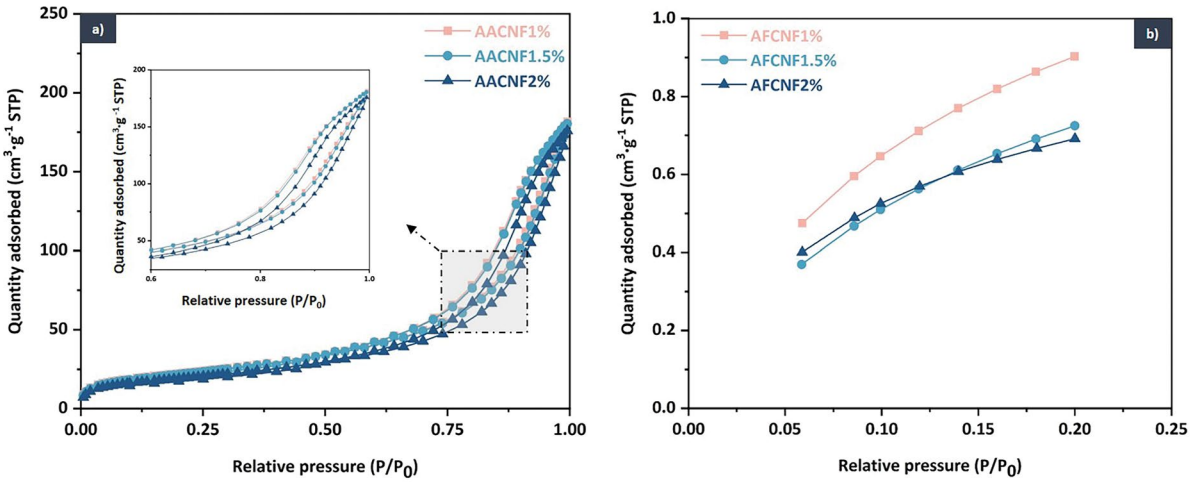

Fig. 2 Isotherms of cellulose nanofiber aerogels: **a** N_2 adsorption/desorption isotherms of CNF aerogels synthesis via acetone supercritical CO_2 drying method and **b** Kr adsorption isotherms of CNF aerogels synthesis via freeze-drying process

out by adsorption-desorption analysis. Nitrogen (N_2) adsorption/desorption isotherms of CNF aerogels prepared via acetone Sc–CO_2 drying are presented in Fig. 2a. For aerogels obtained by freeze-drying, krypton adsorption isotherms are shown in Fig. 2b. The use of krypton as an adsorption gas is motivated by its higher charge density and greater interaction with the nanofiber surfaces, enabling more accurate measurements, particularly for relatively small specific surface areas (i.e. as in the case of nanocellulose aerogels prepared by freeze-drying). These isotherms illustrate the trends observed for all the aerogels prepared by different drying techniques. Other isotherms are reported in the supplementary information.

The aerogels prepared via supercritical drying exhibited similar N_2 adsorption-desorption isotherms. According to the classification of the International Union of Pure and Applied Chemistry (IUPAC), these isotherms are of type II with a type H3 hysteresis loop (Zhang et al. 2016). This suggests that the aerogels exhibit a relatively narrow pore distribution, with a significant increase in adsorption at high pressures. It is also indicating the presence of well-developed macrospores. The appearance of hysteresis during desorption is linked to the presence of narrow-entry pores. During adsorption, the gas molecules rapidly enter the pores, but during desorption, they tend to remain trapped for longer time due to surface interactions resulting in capillary condensation. The krypton adsorption isotherms do not follow any type of isotherm classified according to IUPAC. These isotherms follow an inverse exponential curve with a rapid increase in adsorption, suggesting the presence of macroporous structure.

The specific surface area and pore volume of nanocellulose aerogels, estimated from adsorption isotherms, are summarized in Table 3. The aerogel properties were greatly affected by the initial concentration of nanofibers in the hydrogel and the drying method. For aerogels prepared by supercritical drying, a decrease in the specific surface area is observed with increasing nanofibers concentration. This decrease is linked to a higher rate of interactions, thickening pore walls and thus reducing specific surface area and pore volume (Ciftci et al. 2017). Nevertheless, these specific surface areas remain lower than those reported in previous studies (Ciftci et al. 2017; Sepahvand et al. 2020). This difference is linked to the hydrogel formation process. Hydrogels are formed via physical cross-links induced by hydrogen bonds. These bonds are generated by a freeze-thaw process of the nanofiber suspensions. However, this freezing process is relatively slow, allowing the ice crystals to grow to significant sizes, sometimes tens or hundreds of micrometers. Consequently, the growth of ice crystals has a significant impact on the size of the pores formed in the three-dimensional structure of hydrogels. So, although supercritical drying enables water to be removed from hydrogels without

deforming the microstructure, the size of the ice crystals formed during freezing limits the final porosity and specific surface area of the aerogels obtained.

Comparing the effect of solvent on variations in the specific surface area, there is only slight fluctuation for aerogels containing 2 wt.% nanofibers, with a slight increase observed for aerogels that have undergone solvent exchange using acetone. However, a marked variation is observed for aerogels with low nanofiber concentration. Solvent exchange with acetone resulted in a significant reduction in the shrinkage rate, leading to a significant increase in the specific surface area. Regarding the effect of lignin, a similar tendency is observed with a decrease in the specific surface area with increasing lignocellulose nanofiber concentration. Despite the weak interactions between LCNFs, a higher specific surface area was expected compared to the lignin-free aerogels. However, this small variation can be attributed to more pronounced shrinkage during the drying process.

The specific surface area of freeze-dried aerogels was relatively low, around ten times lower than those obtained from supercritically dried aerogels. The S_{BET} of less than 5 m^2/g does not necessarily suggest the absence of pores but rather suggests that the existing pores are relatively large or the porous structure is not highly developed (Ciftci et al. 2017). This is likely attributed to the destruction of the pore structure by the sublimation of water crystals during the drying process (Buchtová and Budtova 2016).

Aerogels microstructure

The cross-sectional microstructures of aerogels, elaborated using two different drying methods, are shown in the scanning electron microscopy (SEM) images in Fig. 3. Longitudinal sections reveal honeycomb-shaped matrices, where irregular pores are aligned and framed by walls made of nanofibers arranged in films. This interconnected structure offering a diversity of pore sizes with sheet-like pore walls, is observed in both drying methods. In contrast to the general trend for nanocellulose aerogels prepared by supercritical drying, which often feature a network of small and corrugated beads assembled together (Buchtová et al. 2019), the microstructures obtained here stem from the ice crystal growth during hydrogel formation. In this study, nanocellulose hydrogels were formed by a physical cross-linking method involving freeze-thawing. Thus, the pores replicate the shape of ice crystals, creating this layered porous structure that persists even using supercritical drying. Nevertheless, a slight difference can be observed in terms of pore sizes. Indeed, for aerogels that have undergone supercritical drying, a range of pore size from meso- to macropore can be observed. On the other hand, freeze-dried aerogels show macropores and large "open channels". This disparity may be explained by the fact that the latter undergoes secondary freezing prior to freeze-drying. During this second freezing, the formation of ice crystals disturbs the nanostructure of the hydrogels by “pressing” the cellulose nanofibers against the pore walls. This phenomenon partially destroys the initial three-dimensional

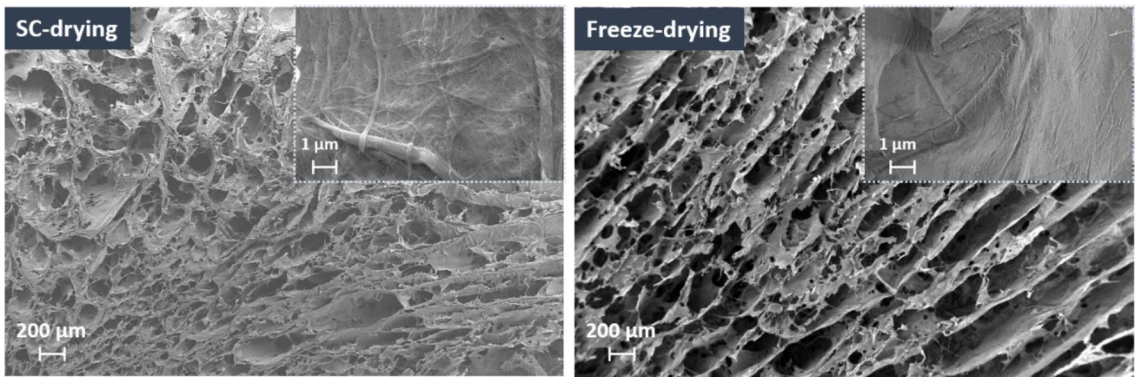

Fig. 3 SEM images of the cross-sectional microstructure of aerogels, elaborated using two different drying methods

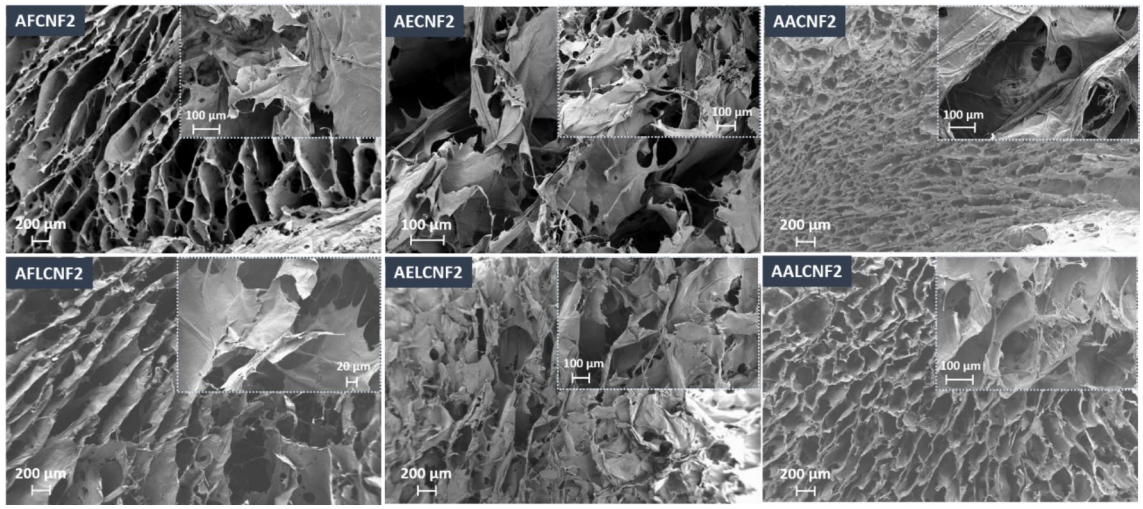

Fig. 4 SEM images of 2 wt.% nanocellulose-based aerogels synthesis by different drying methods

network, resulting in larger and less homogeneous structures, which is consistent with the observations made in previous works (Wang et al. 2017; Chen et al. 2019). At higher magnification, this alteration also affects the distribution of nanofibers. In freeze-dried aerogels, the nanofibers tend to form highly aggregated structures, resulting in a flat surface without pores. Conversely, SC-dried aerogels exhibit less aggregation among nanofibers, creating a surface with mesopores.

The aerogels shown in Fig. 4 are based on nanocellulose with the similar nanofiber concentration (2 wt.%). The presence of lignin in nanocellulose aerogels induces substantial changes in their microstructure. At higher magnification, observation reveals significant differences between the pore walls of aerogels composed of cellulose nanofibers and those containing lignin. Pore walls appear ultra-smooth and thicker in the case of CNF-based aerogels, while less smooth walls are discernible on LCNF-based aerogels. This distinction is particularly noticeable for microstructures of aerogels with lower concentrations, as illustrated in Fig. S3. Moreover, as the nanofiber concentration increases, the microstructures become denser with a consequent increase in the pore wall thickness resulting from intensified nanofiber interactions. When the solvent is exchanged using acetone, a slight increase in the pore density is observed compared to the supercritical drying with ethanol solvent exchange. This variation underlines the complexity of the factors to be considered when designing nanocellulose aerogels.

Mechanical properties

Uniaxial compression tests were carried out to evaluate the mechanical properties of the nanocellulose-based aerogels. The stress-strain curves obtained for nanocellulose-based aerogels prepared via acetone supercritical CO_2 drying are shown in Fig. 4, and similar results were observed for all the other aerogels examined (supporting information). Compression tests were carried out only on aerogels with nanofiber mass fractions of 1.5 wt.% and 2 wt.% for the aerogels synthesized by supercritical drying. Aerogels with lower nanofiber concentrations could not be tested due to their irregular shape attributed to the more pronounced shrinkage during the drying process. On first appearance, these nanocellulose-based aerogels, made up of intertwined nanofibers, show high flexibility while exhibiting considerable ductility compared to regular organic aerogels.

From a qualitative perspective, the stress-strain curves reveal three distinct phases. Initially, a linear region is observed at low deformations, extending up to approximately 15% strain. This phase, from where the compression modulus E is determined, is attributed to the elastic deformation of the cell wall and the collapse of macropores (Ganesan et al. 2016). Subsequently, the curve gradually flattens between

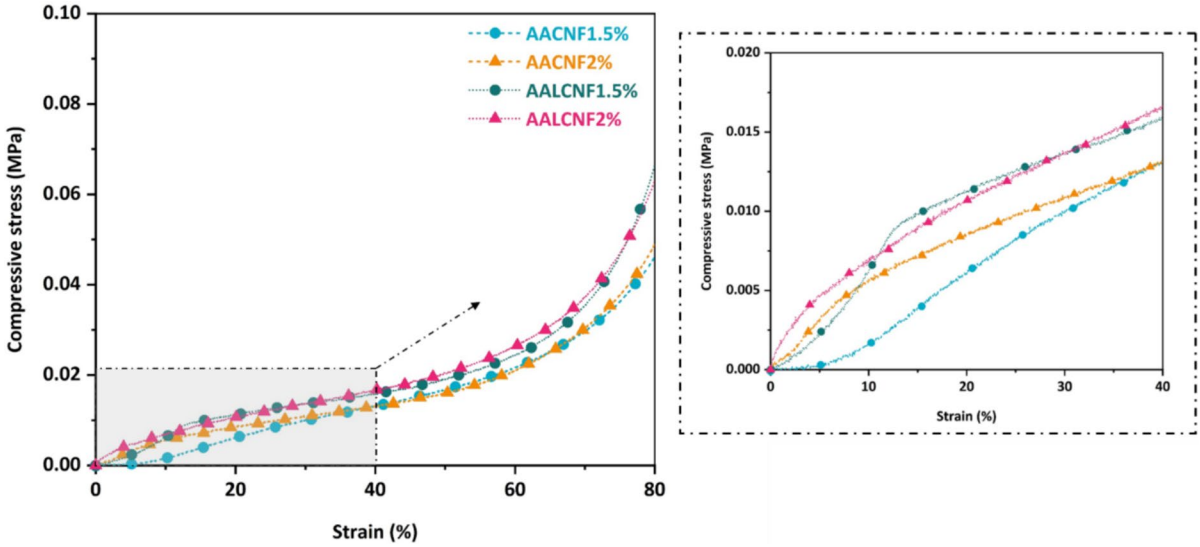

Fig. 5 Strain–stress curves of nanocellulose-based aerogels synthesized via freeze-drying process

Table 4 Young's modulus of nanocellulose-based aerogels

Sample	Nanocellulose concentration (wt.%)	Young's modulus (MPa)
AACNF	1	–
	1.5	0.2113
	2	0.3570
AALCNF	1	–
	1.5	0.2938
	2	0.3817
AECNF	1	–
	1.5	0.1424
	2	0.2812
AELCNF	1	–
	1.5	0.2415
	2	0.4725
AFCNF	1	0.1034
	15	0.2638
	2	0.3006
AFLCNF	1	0.1292
	1.5	0.2701
	2	0.3854

15% and 60% strain, with a more moderate increase in stress resulting from the plastic deformation of cell walls. In the third region (between 60% and 80% strain deformation), the significant increase in stress is induced by densification due to bending or damage to mesopores, as well as compression and rupture of covalent bonds between the cellulose nanofibers, as illustrated in Fig. 5.

The Young's modulus of nanocellulose-based aerogels is reported in Table 4. It can be observed that the mass content of nanofibers in aerogels correlates directly with their compressive modulus. By increasing the initial nanofiber concentration from 1.5 to 2 wt.%, the modulus of AACNF aerogels increases from 0.2113 to 0.3570 MPa. In fact, with increasing nanocellulose mass fraction, the number of cross-linking points increased, making the aerogel more compact and thus increasing the compressive strength. This tendency is observed for both types of porous nanocellulose materials investigated. Notably, these results clearly surpass those reported by (Morcillo-Martín et al. 2022). Although the aerogels were synthesized by two different drying modes (supercritical drying and freeze-drying) that lead to distinct specific surface areas, they exhibit fairly similar compressive moduli. This consistency can be explained by the similar morphology of the different materials, observable in the microstructures obtained by SEM. All aerogels presented a sheet-like microstructure, conferring good resistance under compressive stress. Regarding the effect of the lignin, the aerogels containing lignin showed superior properties to those made from CNFs. The presence of lignin provides the

aerogels with higher mechanical properties, underlining its beneficial role in strengthening these materials.

Effects of lignin on the properties of nanocellulose-based aerogels

By incorporating lignin into cellulose nanofibers, several properties of the aerogels were significantly affected. From a visual standpoint, lignin-containing hydrogels exhibit a distinct brownish colour, attributable to the aromatic compounds of lignin (Berglund et al. 2018). In addition, these hydrogels undergo noticeable shrinkage during drying, which is linked to the reduced rigidity of the resulting hydrogel network.

The hydrophobic nature of lignin plays a crucial role in the formation of the three-dimensional hydrogel network. Lignin-containing nanocellulose fibers create zones where interfibrillar interactions are limited due to the non-polar hydrocarbon compounds and benzene groups (Ciolacu et al. 2012). These reduce interactions contribute to a decrease in the number of cross-linking points and weaken the formation of hydrogen bonds which is essential for the rigidity and cohesion of the hydrogel network. Consequently, a less rigid network is formed, thus inducing more pronounced shrinkage during supercritical drying. The pronounced aerogel shrinkage during drying generates greater compression of the aerogel structure as observed in Fig. 6b. In turn, the compression reducing the space between the nanofibers tends to increase the bulk density of the LCNF aerogels.

Lignin also has an effect on the aerogel's porosity. LCNFs, impregnated with the rich complexity of lignin, exhibit a distinct structure and hydrophobicity compared to their lignin-free counterparts (CNFs). This singularity promotes a reduced number of cross-linking points. Indeed, this configuration generates less regular and larger pores in the resulting aerogel's structure. This phenomenon leads to a reduced porosity but significantly increases the pore volume in the lignocellulose-based aerogels. This notable disparity in the pore structure is highlighted by the

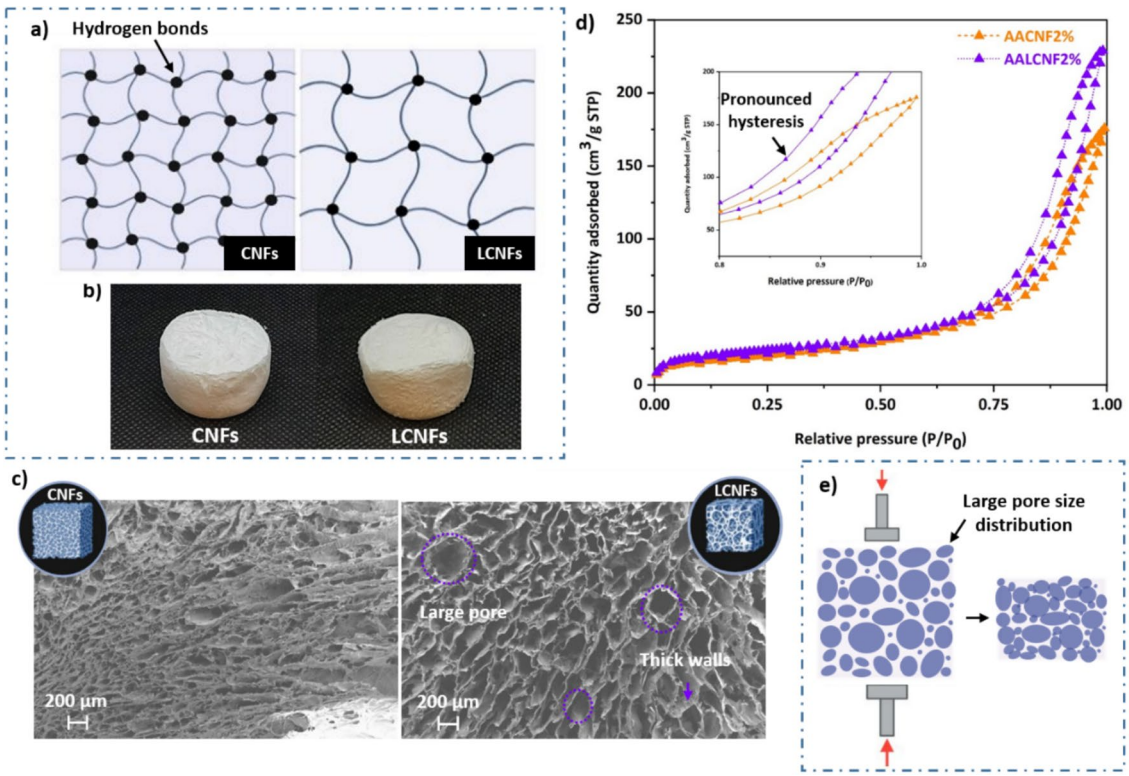

Fig. 6 Schematic illustrations of lignin's impact on nanocellulose-based aerogels: **a** three-dimensional hydrogel network formation, **b** aerogel appearance and shrinkage rate, **c** microstructure alterations, **d** specific surface area enhancement, **e** mechanical properties

SEM micrographs reported in Fig. 6c. LCNF aerogels exhibit a larger pore size distribution, with a predominance of large pores and highly branched irregular walls (McDonagh and Chinga-Carrasco 2020). This structure induced by the presence of lignin, which creates distinct interaction zones that modify pore formation and arrangement, resulting in a more complex, branched pore structure.

This phenomenon is particularly evident in the specific surface area of the aerogels. In the case of LCNF-based aerogels, despite exhibiting reduced porosity, their intricate pore structure, characterized by a large pore size distribution and a highly branched architecture, significantly enhances the specific surface area per unit mass. Additionally, this large pore size distribution is substantiated by the hysteresis observed in N_2 adsorption-desorption isotherms. The hysteresis loops indicate the presence of narrow entrance and branched pores, which are more pronounced in the isotherms of LCNF aerogels, as highlighted in Fig. 6d, which provides a close-up of the hysteresis region. This pronounced hysteresis underscores the complexity of their pore structure, contributing to a higher specific surface area.

In terms of mechanical properties, LCNF-based aerogels exhibit a higher compressive modulus than their CNF-based counterparts. This improvement in mechanical strength stems from the unique characteristics conferred by the presence of lignin. Lignin, known for its intrinsic rigidity and complex aromatic structure, significantly strengthens the structural network of aerogels (Herrera et al. 2018).

In addition, during the formation of LCNF-based aerogels, lignin adds an extra dimension due to its hydrophobic nature and complex structure, resulting in a large pore size distribution and thicker walls. This complex configuration offers increased resistance to compressive stress. In fact, as the initial linear elasticity region of stress-strain curves is caused by the bending of nanofibrils in the open pore space, the elastic modulus of aerogels depends on how the nanofibrils are distributed in the matrix (Ganesan et al. 2019). CNF-based aerogels exhibit interconnected pore structures and when subjected to compressive stress, these structures undergo cell wall collapse. In contrast, LCNF-based aerogels feature thicker cell walls and branched nanofibrillar supports with a wider pore size distribution (Fig. 6e). This robust architecture offers superior compressive strength, providing aerogels with greater structural integrity.

Conclusions

The research underscores the impact of cellulose nanofiber mass composition (1, 1.5 and 2 wt.%), drying method (freeze-drying and supercritical drying), and the presence of lignin on the properties of the nanocellulose-based aerogels. The choice between freeze-drying and supercritical drying significantly shapes aerogel properties, with the former preserving structure and minimizing shrinkage, while the latter yields a higher BET-specific surface area. Scanning electron microscopy analysis reveals honeycomb-shaped matrices with irregular pores, influenced by nanocellulose concentration and drying technique. Uniaxial compression tests demonstrate that nanocellulose aerogels possess notable flexibility and high compressive modulus. The incorporation of lignin into cellulose nanofibers has a significant impact on the aerogels' properties. Hydrogels containing lignin had a brownish color and shrink significantly during drying due to reduced network rigidity and hydrophobic interactions that limit hydrogel cross-linking. This results in larger and more irregular porous structure reducing porosity while increasing pore volume and bulk density. Despite lower porosity, LCNF aerogels exhibit an intricate pore structure with a narrow pore size distribution and highly branched architecture, which substantially increases their specific surface area. Mechanically, lignin-containing nanocellulose aerogels exhibit a higher compressive modulus, attributed to the stiffness and complex structure of the lignin, enhancing their strength and structural integrity. In summary, the study provides insight into the complex relationship between nanocellulose composition, drying methods, and the properties of the aerogels. Cellulose-based aerogels, in particular those incorporating lignin, offer potential for the design of nanocellulose-based materials with properties suitable for a variety of applications.

Acknowledgments The authors would like to thank Antoine Adjaoud, Danny Bialuschewski and Kai Steffens for valuable discussion and experimental assistance.

Author contributions F.B. and K.G.: data curation; investigation; methodology; writing original draft, F.B.: prepared

figures 1, 2, 5 and 6, F.B., K.G., B.M. and J.L.: investigation, B.M. and J.L.: supervision; review & editing.

Funding Open Access funding provided thanks to the CRUE-CSIC agreement with Springer Nature. This work was financially supported by the University of the Basque Country (grant PIF21/52) and Basque Government (IT1498-22).

Data availability Data is provided within the manuscript or supplementary information files.

Declarations

Conflict of interest The authors declare no competing interests.

Ethical approval Not applicable.

Consent for publication All authors agree to publish this work.

References

Adjaoud A, Dieden R, Verge P (2021) Sustainable esterification of a soda lignin with phloretic acid. Polymers (Basel) 13:637. https://doi.org/10.3390/polym13040637

Baraka F, Robles E, Labidi J (2023) Microwave-assisted esterification of bleached and unbleached cellulose nanofibers. Ind Crops Prod 191:115970. https://doi.org/10.1016/j.indcrop.2022.115970

Berglund L, Forsberg F, Jonoobi M, Oksman K (2018) Promoted hydrogel formation of lignin-containing arabinoxylan aerogel using cellulose nanofibers as a functional biomaterial. RSC Adv 8:38219–38228. https://doi.org/10.1039/C8RA08166B

Buchtová N, Budtova T (2016) Cellulose aero-, cryo- and xerogels: towards understanding of morphology control. Cellulose 23:2585–2595. https://doi.org/10.1007/s10570-016-0960-8

Buchtová N, Pradille C, Bouvard J-L, Budtova T (2019) Mechanical properties of cellulose aerogels and cryogels. Soft Matter 15:7901–7908. https://doi.org/10.1039/C9SM01028A

Chen H-B, Wang Y-Z, Schiraldi DA (2013) Foam-like materials based on whey protein isolate. Eur Polym J 49:3387–3391. https://doi.org/10.1016/j.eurpolymj.2013.07.019

Chen Y, Zhou L, Chen L et al (2019) Anisotropic nanocellulose aerogels with ordered structures fabricated by directional freeze-drying for fast liquid transport. Cellulose 26:6653–6667. https://doi.org/10.1007/s10570-019-02557-z

Chen Y, Zhang L, Yang Y et al (2021) Recent progress on nanocellulose aerogels: preparation, modification, composite fabrication applications. Adv Mater 33:2005569. https://doi.org/10.1002/adma.202005569

Ciftci D, Ubeyitogullari A, Huerta RR et al (2017) Lupin hull cellulose nanofiber aerogel preparation by supercritical CO_2 and freeze drying. J Supercrit Fluids 127:137–145. https://doi.org/10.1016/j.supflu.2017.04.002

Ciolacu D, Oprea AM, Anghel N et al (2012) New cellulose–lignin hydrogels and their application in controlled release of polyphenols. Mater Sci Eng C 32:452–463. https://doi.org/10.1016/j.msec.2011.11.018

Daicho K, Kobayashi K, Fujisawa S, Saito T (2020) Crystallinity-independent yet modification-dependent true density of nanocellulose. Biomacromol 21:939–945. https://doi.org/10.1021/acs.biomac.9b01584

De France KJ, Hoare T, Cranston ED (2017) Review of hydrogels and aerogels containing nanocellulose. Chem Mater 29:4609–4631. https://doi.org/10.1021/acs.chemmater.7b00531

Dufresne A (2019) Nanocellulose processing properties and potential applications. Curr for Rep 5:76–89. https://doi.org/10.1007/s40725-019-00088-1

Fu L, Fang Z, Chen H et al (2022) Production of lignocellulose nanofibril (LCNF) from high yield pulps by hydrated deep eutectic solvents (DES) pretreatment for fabricating biobased straw. Ind Crops Prod 188:115738. https://doi.org/10.1016/j.indcrop.2022.115738

Ganesan K, Dennstedt A, Barowski A, Ratke L (2016) Design of aerogels, cryogels and xerogels of cellulose with hierarchical porous structures. Mater Des 92:345–355. https://doi.org/10.1016/j.matdes.2015.12.041

Ganesan K, Barowski A, Ratke L, Milow B (2019) Influence of hierarchical porous structures on the mechanical properties of cellulose aerogels. J Sol-Gel Sci Technol 89:156–165. https://doi.org/10.1007/s10971-018-4828-2

García-González CA, Alnaief M, Smirnova I (2011) Polysaccharide-based aerogels–promising biodegradable carriers for drug delivery systems–review article. Carbohydr Polym 86:1425–1438. https://doi.org/10.1016/j.carbpol.2011.06.066

García-González CA, Camino-Rey MC, Alnaief M et al (2012) Supercritical drying of aerogels using CO_2: effect of extraction time on the end material textural properties. J Supercrit Fluids 66:297–306. https://doi.org/10.1016/j.supflu.2012.02.026

García-González CA, Jin M, Gerth J et al (2015) Polysaccharide-based aerogel microspheres for oral drug delivery. Carbohydr Polym 117:797–806. https://doi.org/10.1016/j.carbpol.2014.10.045

Herrera M, Thitiwutthisakul K, Yang X et al (2018) Preparation and evaluation of high-lignin content cellulose

nanofibrils from eucalyptus pulp. Cellulose 25:3121–3133. https://doi.org/10.1007/s10570-018-1764-9
Ho NAD, Leo CP (2021) A review on the emerging applications of cellulose, cellulose derivatives and nanocellulose in carbon capture. Environ Res 197:111100. https://doi.org/10.1016/j.envres.2021.111100
Husain FM, Khan A, Khan RA et al (2021) Chapter 18–bio-based aerogels and their environment applications: an overview. In: Khan AAP, Ansari MO, Khan A (eds) Advances in aerogel composites for environmental remediation. Elsevier, Amsterdam, pp 347–356
Illera D, Mesa J, Gomez H, Maury H (2018) Cellulose aerogels for thermal insulation in buildings: trends and challenges. Coatings 8:345
Jiang J, Zhu Y, Jiang F (2021) Sustainable isolation of nanocellulose from cellulose and lignocellulosic feedstocks: recent progress and perspectives. Carbohydr Polym 267:118188. https://doi.org/10.1016/j.carbpol.2021.118188
Kargarzadeh H, Mariano M, Gopakumar D et al (2018) Advances in cellulose nanomaterials. Cellulose 25:2151–2189. https://doi.org/10.1007/s10570-018-1723-5
Keshavarz L, Ghaani MR, MacElroy JMD, English NJ (2021) A comprehensive review on the application of aerogels in CO_2-adsorption: materials and characterisation. Chem Eng J 412:128604. https://doi.org/10.1016/j.cej.2021.128604
Kistler SS (1931) Coherent expanded aerogels and jellies. Nature 127:741. https://doi.org/10.1038/127741a0
Liu K, Du H, Zheng T et al (2021) Lignin-containing cellulose nanomaterials: preparation and applications. Green Chem 23:9723–9746. https://doi.org/10.1039/D1GC02841C
Mankar AR, Pandey A, Modak A, Pant KK (2021) Pretreatment of lignocellulosic biomass: a review on recent advances. Bioresour Technol 334:125235. https://doi.org/10.1016/j.biortech.2021.125235
McDonagh BH, Chinga-Carrasco G (2020) Characterization of porous structures of cellulose nanofibrils loaded with salicylic acid. Polymers (Basel) 12:2538
Morales A, Labidi J, Gullón Estévez P (2021) Impact of the lignin type and source on the characteristics of physical lignin hydrogels. Sustain Mater Technol 31:e00369. https://doi.org/10.1016/j.susmat.2021.e00369
Morcillo-Martín R, Espinosa E, Rabasco-Vílchez L et al (2022) Cellulose nanofiber-based aerogels from wheat straw: influence of surface load and lignin content on their properties and dye removal capacity. Biomolecules 12:232
Pääkkö M, Vapaavuori J, Silvennoinen R et al (2008) Long and entangled native cellulose I nanofibers allow flexible aerogels and hierarchically porous templates for functionalities. Soft Matter 4:2492–2499. https://doi.org/10.1039/B810371B
Park S, Baker J, Himmel M et al (2010) Cellulose crystallinity index: measurement techniques and their impact on interpreting cellulase performance. Biotech Biofuels 3:10. https://doi.org/10.1186/1754-6834-3-10
Pierre AC, Pajonk GM (2002) Chemistry of aerogels and their applications. Chem Rev 102:4243–4266. https://doi.org/10.1021/cr0101306
Raman SP, Keil C, Dieringer P et al (2019) Alginate aerogels carrying calcium, zinc and silver cations for wound care: fabrication and metal detection. J Supercrit Fluids 153:104545. https://doi.org/10.1016/j.supflu.2019.104545
Rojo E, Peresin MS, Sampson WW et al (2015) Comprehensive elucidation of the effect of residual lignin on the physical, barrier, mechanical and surface properties of nanocellulose films. Green Chem 17:1853–1866. https://doi.org/10.1039/C4GC02398F
Sepahvand S, Jonoobi M, Ashori A et al (2020) A promising process to modify cellulose nanofibers for carbon dioxide (CO_2) adsorption. Carbohydr Polym 230:115571. https://doi.org/10.1016/j.carbpol.2019.115571
Sepahvand S, Kargarzadeh H, Jonoobi M et al (2023) Recent developments in nanocellulose-based aerogels as air filters: a review. Int J Biol Macromol 246:125721. https://doi.org/10.1016/j.ijbiomac.2023.125721
Steiner S, Anderson A, Brock S et al (2023) Recipes and designs for aerogels. Springer, Cham, pp 1643–1728
Tafreshi OA, Mosanenzadeh SG, Karamikamkar S et al (2022) A review on multifunctional aerogel fibers: processing, fabrication, functionalization, and applications. Mater Today Chem 23:100736. https://doi.org/10.1016/j.mtchem.2021.100736
Tanguy NR, Wu H, Nair SS et al (2021) Lignin cellulose nanofibrils as an electrochemically functional component for high-performance and flexible supercapacitor electrodes. Chemsuschem 14:1057–1067. https://doi.org/10.1002/cssc.202002558
Verma A, Thakur S, Goel G et al (2020) Bio-based sustainable aerogels: new sensation in CO_2 capture. Curr Res Green Sustain Chem 3:100027. https://doi.org/10.1016/j.crgsc.2020.100027
Visanko M, Sirviö JA, Piltonen P et al (2017) Mechanical fabrication of high-strength and redispersible wood nanofibers from unbleached groundwood pulp. Cellulose 24:4173–4187. https://doi.org/10.1007/s10570-017-1406-7
Wang M, Shao C, Zhou S et al (2017) Preparation of carbon aerogels from TEMPO-oxidized cellulose nanofibers for organic solvents absorption. RSC Adv 7:38220–38230. https://doi.org/10.1039/C7RA05506D
Wang Y, Su Y, Wang W et al (2019) The advances of polysaccharide-based aerogels: Preparation and potential application. Carbohydr Polym 226:115242. https://doi.org/10.1016/j.carbpol.2019.115242
Wei J, Geng S, Hedlund J, Oksman K (2020) Lightweight, flexible, and multifunctional anisotropic nanocellulose-based aerogels for CO_2 adsorption. Cellulose 27:2695–2707. https://doi.org/10.1007/s10570-019-02935-7
Zhang Y, Shao D, Yan J et al (2016) The pore size distribution and its relationship with shale gas capacity in organic-rich mudstone of Wufeng-Longmaxi formations, Sichuan Basin, China. J Nat Gas Geosci 1:213–220. https://doi.org/10.1016/j.jnggs.2016.08.002
Zhu W, Zhang Y, Wang X et al (2021) Preparation and comparative study of aerogels based on cellulose nanocrystals and nanofibers from eucalyptus pulp